IEEE Access
Multidisciplinary ⋮ Rapid Review ⋮ Open Access Journal

Received January 18, 2021, accepted January 20, 2021, date of publication January 25, 2021, date of current version February 2, 2021.

Digital Object Identifier 10.1109/ACCESS.2021.3054019

Electromagnetic Interference Inside the Control System Cabinet of a Nuclear Power Plant From External Wireless Devices

JONG-EON PARK[1] AND HOSUNG CHOO[2], (Senior Member, IEEE)
[1]Division of Navigation Convergence, Korea Maritime and Ocean University, Busan 49112, South Korea
[2]School of Electronic and Electrical Engineering, Hongik University, Seoul 04066, South Korea

Corresponding author: Hosung Choo (hschoo@hongik.ac.kr)

This work was supported by the Dongguk University Research Fund of 2020.

ABSTRACT This article investigates the scattering characteristics inside the cabinet of a nuclear power plant by the mode-matching technique (MMT) when arbitrary wireless devices are assumed to be applied in the plant. The modal decomposition, multiregion problem, and power conservations of the MMT are introduced to confirm the scattered field inside the cabinet. It is found that stronger scattered fields are usually found when the center of the gap in the rear door of the cabinet is located $1.5\lambda_0$ away from the side wall. Therefore, when determining the geometry of the cabinet and digital modules, the scattered field inside the cabinet is systematically analyzed in advance, and appropriate design guidelines for the cabinet can be suggested.

INDEX TERMS Electromagnetic compatibility, electromagnetic interference, mode-matching technique, multiregion problem.

I. INTRODUCTION

The use of wireless devices or communication systems in nuclear power plants (NPPs) has been gradually increasing because of the advantages of low wiring costs, convenience of maintenance, easy mobility, etc. [1], [2]. Before applying wireless devices in an indoor NPP environment, however, it is necessary to carry out preliminary tests to ensure unwanted electromagnetic fields from wireless devices do not affect the digital modules inside the cabinet of an NPP. Therefore, when an arbitrary electromagnetic field is incident into the cabinet, the electromagnetic scattering characteristics around the digital modules should be thoroughly investigated [3], [4].

Several research results of the electromagnetic scattering phenomena inside the cabinet of an NPP are investigated in [5]–[8]. The scattered field inside the cabinet can be obtained by various numerical techniques [9]–[11], such as finite-difference time-domain method, finite element method, or method of moments. However, the mode-matching technique (MMT) is one of the appropriate numerical techniques to solve reflection and transmission characteristics at the discontinuities because the various modal propagations provide a better understanding of the electromagnetic interference inside the cabinet. In addition, when compared to other computational methods, the MMT generally does not require large computational capacity. For the MMT, the scattered fields are obtained in one or two minutes if the geometry description for the cabinet was already set up. However, the simulation results for the commercial software such as FEKO simulator takes at least 30 minutes, which are commonly supported by Intel Core *i*7 CPU @ 2.80 GHz and 16 GB RAM. Therefore, once an initial description is fully set up, various scattered fields can be obtained immediately by slightly changing the cabinet geometry thanks to the MMT.

Nevertheless, previous research [5], [6], [8] is limited to cases where a too simplified bundle of digital modules is applied or the rear door of the cabinet is usually closed. In practice, however, dozens of digital modules are placed separately in the cabinet, and the rear doors usually have small openings for the passage of cables required to supply electric power or connect the other instruments in the adjacent cabinets.

The main features of this paper can be summarized as follows: (1) Novelty - The most important point is to analyze the more complicated interior structure of the cabinet. The previous studies [4], [6] simply analyzed the scattered electromagnetic fields for a single bundle of digital modules,

The associate editor coordinating the review of this manuscript and approving it for publication was Wenjie Feng.

when a rear door is closed. In this study, however, separated three and separated four digital modules were considered. Moreover, the opening of the rear door was also considered for the analysis. (2) Computational approach - The results of these kind of studies are usually analyzed by a commercial simulator, but this study applied the 'MMT'. The advantage of applying the MMT is to understand the transmission physics for each mode as well as entire field distributions. (3) Application (Research necessity) - When there are 'multiple' digital modules and the rear door is 'partially open', the maximum and minimum scattered fields can be found. Therefore, the guidelines can be presented, such as arrangement of digital modules or opening position of the rear door.

In this article, the electromagnetic scattering phenomena around the digital modules inside the cabinet of an NPP are investigated when an arbitrary electromagnetic field is incident from the outside of the cabinet, the arrangement of the digital modules is close to the actual layout, and there is a small opening in the rear door of the cabinet. To compute the scattered field inside the cabinet by the MMT, a parallel-plate waveguide (PPW) is employed to model the digital modules arranged in parallel, and the corresponding modes in each region are obtained in advance. The dimensions of the digital modules and the inside of the cabinet are similar to the actual geometry of the cabinet. Field distributions are investigated when the number of digital modules inside the cabinet is even and odd. The scattered fields around the digital modules are also studied according to the position and width of the opening in the rear door, as well as the number of digital modules. Finally, the scattered fields inside the cabinet using the MMT are verified against the results produced by commercial software.

II. INSIDE GEOMETRY OF THE CABINET AND MMT FORMULATION

A. GEOMETRY OF THE CABINET AND INNER DIGITAL MODULES

Fig. 1(a) shows a front view of the arrays of digital modules in the metallic frame with open cabinet. Fig. 1(b) illustrates a top view of the cabinet with an open front door, including digital instrumentation and control devices (in other words, digital modules) inside the cabinet, which is installed in the NPP. The digital modules are installed inside the cabinet and arranged in parallel along the x-axis. The walls of the cabinet and the digital modules are usually made of metal; therefore, they can be considered a perfect electric conductor (PEC) in the microwave range 2.4–5.0 GHz, which are the application frequencies for wireless local area networks. As shown in Fig. 1, Region 1 is the free space from which the incident wave enters, and Region 2 is the open front door of the cabinet. An electromagnetic wave with parallel polarization is excited from Region 1 to Region 2. (The analyses of the perpendicular polarization case are referred to [5].) On the contrary, there is a small opening in the rear door of Region 6, because bundles of power or signal cables need to pass through the gap. The gap width and position of the rear door could be used as variables to specifically investigate the electromagnetic scattered fields inside the cabinet. Meanwhile, the cables are usually housed in a shielding metallic box in the cabinet, so the effect of bundles of cables could be ignored. The height of the cabinet and digital modules in the y-axis is approximately 2 m, but here it is assumed to be infinite along the y-axis, because it is sufficiently long for the wavelength at 5 GHz, which is the frequency of interest. There are plastic panels in front of the digital modules with a dielectric constant of $2 \sim 3$, however, its influence was not significant, and therefore they were ignored. Figs. 2(a) and (b) show the configurations of the cabinet and digital modules when the number of digital modules is specified as three and four, respectively. The dimensions in the x- and z-axes in Figs. 1 and 2 are presented in Table 1, and each component can be translated into the wavelength at 5 GHz in the final column of Table 1. The gap width and the distance from the right wall to the center of the gap in the rear door are denoted

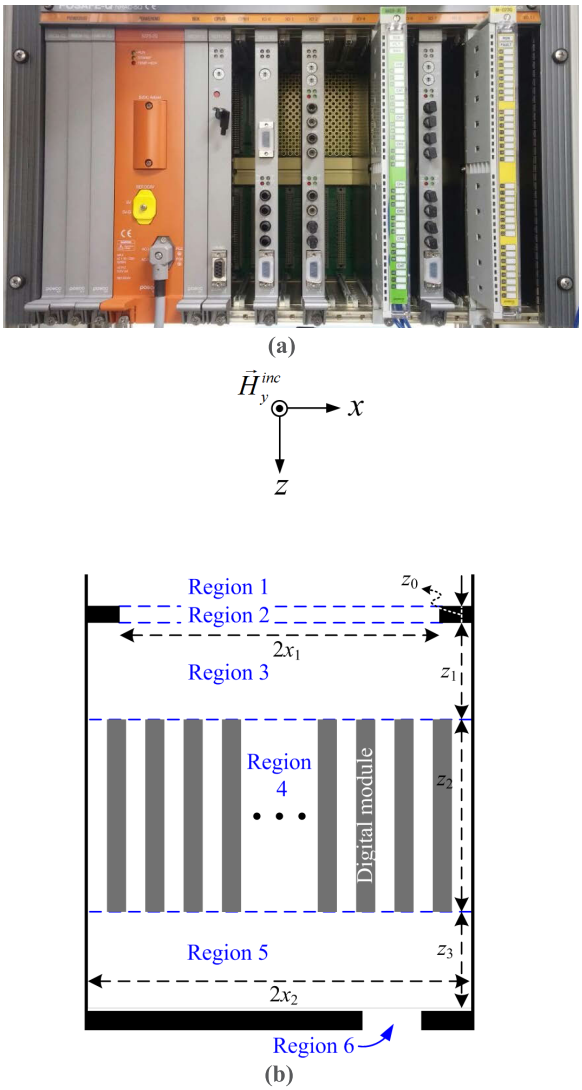

FIGURE 1. The configuration of the cabinet of a nuclear power plant and arrayed digital modules. (a) Photo. (b) The regions inside the cabinet are specified by the numbers from 1 to 6.

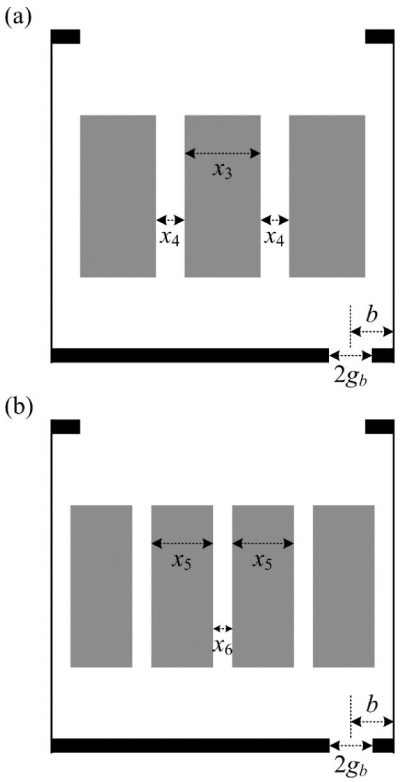

FIGURE 2. The configuration of the cabinet of a nuclear power plant when the number of digital modules is (a) three and (b) four. The widths and spacings of the digital modules are specified. The gap widths and locations of the slot in the rear door of the cabinet are variables.

TABLE 1. Physical dimensions of the cabinet and their electrical lengths at 5.0 GHz.

Dimensions	Physical length [mm]	Electrical length
$2x_1$	600	10 λ_0
$2x_2$	720	12 λ_0
x_3	156	2.6 λ_0
x_4	63	1.05 λ_0
x_5	127.5	2.125 λ_0
x_6	42	0.7 λ_0
z_0	30	0.5 λ_0
z_1	195	3.25 λ_0
z_2	360	6 λ_0
z_3	165	2.75 λ_0

by $2g_b$ and b, respectively, and they are the variables to investigate the electromagnetic field distributions in detail.

Each region in Fig. 1 can be assumed to be a PPW, consisting of two perfectly conducting plates with plate separations such as $2x_1$ and $2x_2$, and the MMT is applied. The H_y-field, instead of the E_y-field, in each region can be arranged [6], because only a parallel-polarized incident wave is considered. The electric fields as well as the H_y-field in the PPW can be obtained, thanks to Maxwell's equation, and the detailed procedure can be referred to [6].

A shielding PEC box surrounding the power cables may be included inside the cabinet. In this case, the region should be considered as the PEC and has to be applied in the MMT formulation. Then, Region 5 in Fig. 1 have to be separated into two regions and formulated by including the modes in the modified region covering the PEC box. It may be considered for a future research topic.

B. MODAL DECOMPOSITION IN REGION 4

The procedure for obtaining the reflection and transmission coefficients from Region 1 to Region 2, and vice versa, was already discussed in [6], and the coefficients at other junctions can be solved in the same manner. However, the modal configuration should be thoroughly considered at the junctions, including Region 4, where four PPWs are assumed to be arranged in parallel. In Region 4, as described in Fig. 3, if an arbitrary mode is assigned to one side of the PPW, zero fields are automatically applied to its other sides. The fields in the areas of the digital modules are zero because the digital modules are assumed to be a PEC. For instance, in Mode 05, the odd TM_1 mode is used for the upper Region 4, and zero fields are formed in other PPWs as well as in the insides of the digital modules. In Mode 06, the odd TM_1 mode is applied in the second PPW of Region 4, and zeros are formed in other regions. Similarly, in Modes 07 and 08, the odd TM_1 modes are located in the third and fourth PPWs in Region 4, respectively. If we assign the modes in this way, the modal orthogonality is exactly satisfied, and the MMT can be employed in our geometry. Eventually, reflection and transmission coefficients for the junctions, including Region 4, can be obtained.

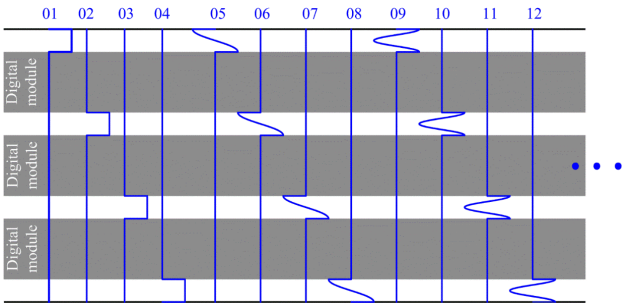

FIGURE 3. The modal decompositions of the first 12 modes in Region 4 from Fig. 2(a).

C. SCATTERING COEFFICIENTS BY THE MMT AND MULTIREGION PROBLEM

The overall solving procedure of the MMT including constructions of the simultaneous equations can be referred to [12]. After obtaining the entire reflection and transmission coefficients for all the junctions, the complete reflection and transmission coefficients for the geometries in Fig. 2 have to be solved [13]. To compute the total coefficients, the multiregion problem should be applied by considering the multiple reflections occurring at the junctions. The specific solving procedure is mentioned in [14] and will not be addressed here.

III. NUMERICAL RESULTS AND DISCUSSIONS

A. POWER CONSERVATION

Power conservation is one of the adequate ways to validate the result of the MMT. In this subsection, the power

conservations at the junctions, including the digital modules in Fig. 2(b), are tested, and we show that the MMT formulations are appropriate. The region of cabinet modules is referred to as Region 4, as shown in Fig. 1. In Region 4, the PPWs are divided into five subregions, and the modes in this region are separated in a similar manner as depicted in Fig. 3. The modes such as even TM_0, odd TM_1, and even TM_2 from Region 3 are excited into Region 4, and the incident power density can be expressed as follows:

$$P_n = \frac{1}{2}\mathrm{Re}\left[\int_{-x_2}^{x_2} (\vec{E}_n \times \vec{H}_n^*)\cdot \vec{dl}\right], \tag{1}$$

where n is the modal index. It is required to calculate the power only along the x-axis, since the geometry assumes that the y-axis in Figure 1 is infinite. If the sum of the reflected and transmitted powers is equal to the nth modal incident power, then the power conservation is proved.

The power densities of the reflected and transmitted waves, including the incident wave, are plotted in terms of the incident modes in Fig. 4, and the power conservation is confirmed for each mode. Junctions 34 and 45 are defined as the boundaries between Regions 3 and 4 and Regions 4 and 5, respectively, and these junctions are depicted in the insets of Figs. 4(a) and (b), respectively. Here, the numbers in the x-axes of Figs. 4 (a) and (b) indicate the modal indices in Regions 3 and 4, respectively, which are explained in Fig. 3. The incident, reflected, and transmitted power densities for each mode are described by the blue asterisks, red inverted triangles, and black circles, respectively. Twenty-four propagating modes are obtained in Region 3, as shown in the x-axis of Fig. 4(a), and the incident power densities for all the modes are calculated with the blue asterisks, according to Eq. (1). After computing the reflection and transmission coefficients from the MMT formulation, the summed reflected and transmitted power densities are achieved by the red triangles and black circles, respectively. The combination of the reflected and transmitted power densities for each mode is almost the same as the incident power density. The difference between the two is only 10^{-12} W/m^2, and it turned out that the power conservation for each mode is completely satisfied. By contrast, the number of propagating modes in Region 4 is only 10, as shown in the x-axis of Fig. 4(b), because there are two propagating modes in each PPW and five separate PPWs in Region 4. In a similar manner, the incident power densities for each mode are calculated in Eq. (1), and the reflected and transmitted power densities for each mode are computed and plotted in Fig. 4(b). It is noteworthy in Fig. 4(b) that the incident waves of the five even TM_0 modes are almost transmitted into Region 5, and few or no mode is reflected back into Region 4. On the contrary, the incident waves of the next five odd TM_1 modes (indices 6–10 in the x-axis) are transmitted mostly into Region 5, and some parts are reflected back into Region 4. In any case, the power conservation at Junction 45 is also satisfied, and the electromagnetic scattering characteristics for each mode can be understood from Fig. 4. The power conservations at other junctions in Fig. 1 are

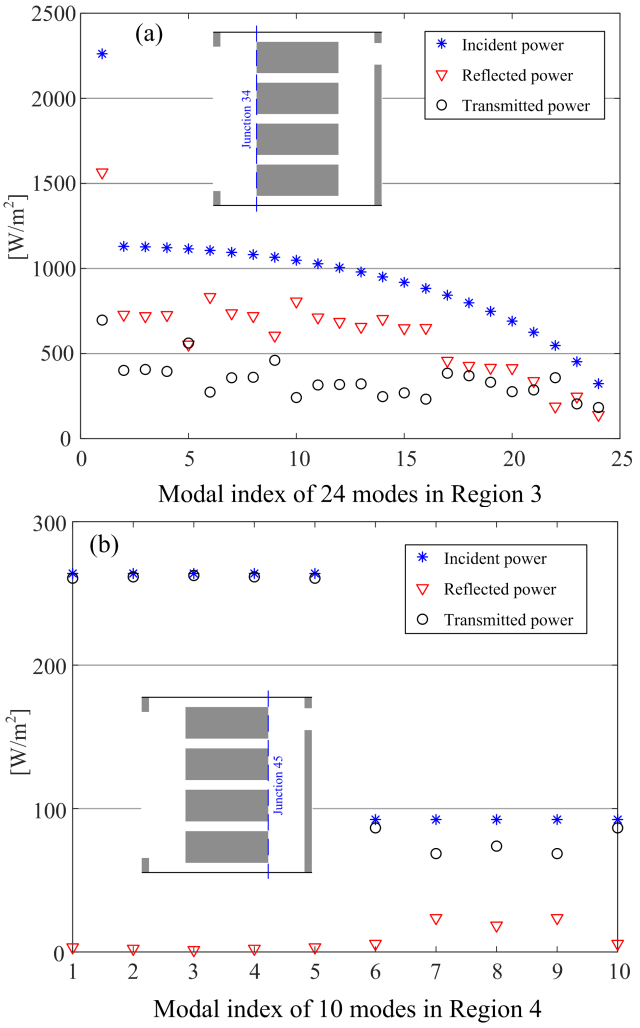

FIGURE 4. The power conservations at (a) Junction 34 and (b) Junction 45. (The inset figures representing the inside of the cabinet are rotated 90 degrees.)

also validated, and the overall reflection and transmission characteristics of the entire geometry of the cabinet are ready to be computed.

B. SCATTERED FIELDS FOR THREE DIGITAL MODULES INSIDE THE CABINET

The scattered fields inside the cabinet are investigated to better understand the field propagating characteristic, when the incident H_y-field is assumed to be 1 A/m. Fig. 5 depicts the scattered fields inside the cabinet as a function of the position of b when there are three digital modules in the cabinet. The opening gap width of $2g_b$ in the rear door is constant at 90 mm. The scattered fields are examined as b is changed from 45 ($0.75\lambda_0$) to 360 mm at intervals of 45 mm. In all eight cases shown in Fig. 5, fluctuations in the z-axis with intervals of $0.5\lambda_0$ are observed because of the standing waves. Especially, the strong standing waves in Region 3 are found in front of the digital modules. The important thing to note here is the changes of the scattered field in Region 4 according to the variable b. There are

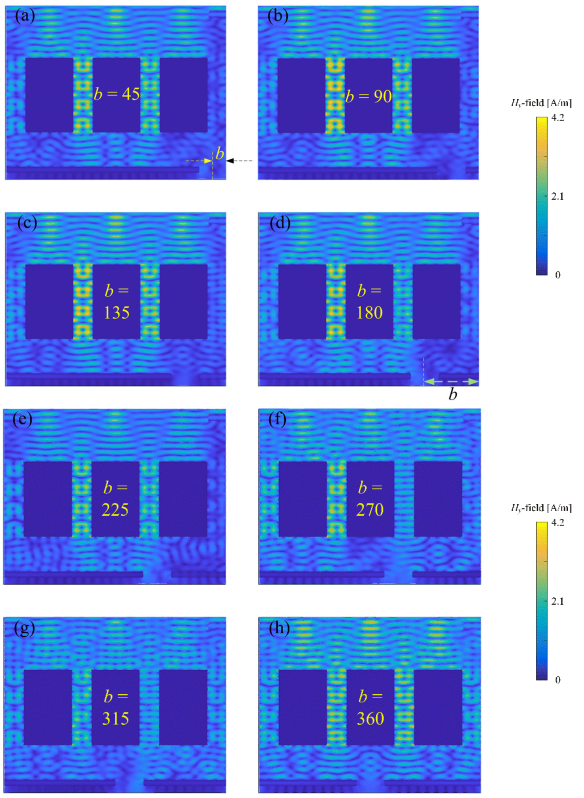

FIGURE 5. H_y-field distributions as a function of variable b (unit: mm) when TM_0 mode is incident, and the number of digital modules is three.

four subregions in Region 4, and strong scattered standing waves are found mainly in two central subregions between the adjacent digital modules. These are observed similarly in Figs. 5(a)–(g), whereas symmetric scattered fields are obtained in the last case of Fig. 5(h) because of the symmetric inside geometry.

To further investigate the scattered field, the strengths of the standing waves in the subregion between the leftmost and central digital modules are studied. Fig. 6(a) shows the H_y-field intensities along the line AB as a function of the gap location b in Region 6, and Fig. 6(b) shows the line AB between the digital modules. Specifically, the strongest H_y-field distribution is obtained when b is 90 mm, and relatively stronger field distributions are achieved when b becomes 135–180 mm. On the contrary, the H_y-field distributions along the line AB become weaker when the gap moves to the center of the rear door, and these are also found in Figs. 5(g) and (h). On the basis of these investigations, the H_y-field distributions in the regions between the adjacent digital modules can be understood and can be useful reference data for the internal design of the cabinet or the allocation of dozens of digital modules.

The H_y-field intensities along the line CD as a function of b are investigated as shown in Fig. 7. As presented in Table 2, the average and maximum H_y-field intensities along the line CD are calculated as a function of b, and relatively larger average H_y-field intensities are found when the locations of b

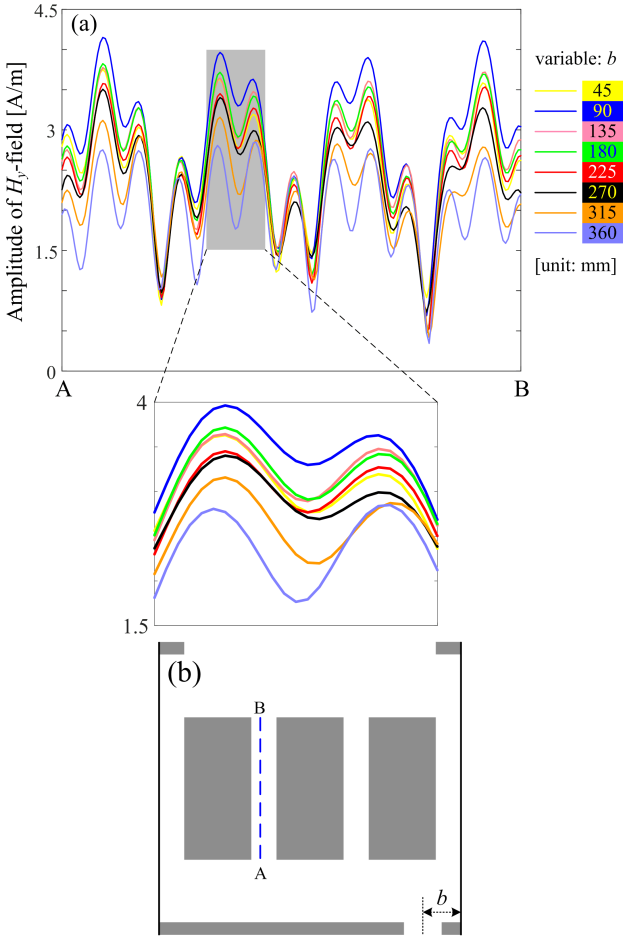

FIGURE 6. The H_y-field strengths along the line AB when b varies from 45 to 360 mm, and three digital modules in the cabinet are considered. (b) The position of the line AB is depicted in the cabinet.

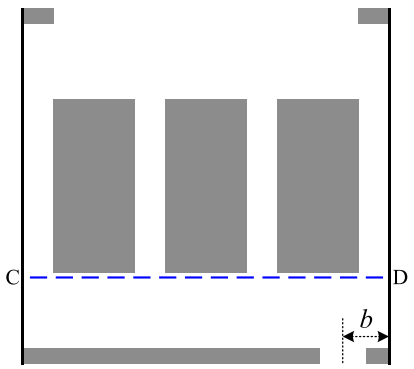

FIGURE 7. The line CD is described in the cabinet, and the H_y-field along the line is examined as a function of b. The average and maximum values along the line are provided in Table 2.

are 315 and 360 mm. At these locations, the transmitted powers through the gap of the rear door become smaller, and relatively stronger standing waves are maintained in Region 5. Meanwhile, the maximum H_y-field intensity is observed when b becomes 90 mm, as given in Table 2. It is understood that the strongest field intensities along the line AB as well as the line CD are found when b is 90 mm.

TABLE 2. Average and maximum H_y -field strengths along the line CD in Fig. 7 with respect to *b*.

b [mm]	Average values [A/m]	Maximum values [A/m]
45	0.966	2.641
90	0.986	2.733
135	0.965	2.478
180	0.998	2.520
225	1.019	2.387
270	1.007	2.511
315	1.175	2.578
360	1.083	2.290

C. SCATTERED FIELDS FOR FOUR DIGITAL MODULES INSIDE THE CABINET

Fig. 8 shows the H_y-field intensities inside the cabinet in the same way as that depicted in Fig. 5, but the number of digital modules is four in this case. Similar to the case of Fig. 5, the scattered field distributions inside the cabinet as a function of the gap location b are described when $2g_b$ is 90 mm. In the same manner, the scattered fields are obtained as b changes from 45 ($0.75\lambda_0$) to 360 mm at 45-mm intervals. Again, in all eight cases shown in Fig. 8, fluctuations along the z-axis are observed at intervals of $0.5\lambda_0$ because of the standing waves. Compared to the case of Fig. 5 (with three digital modules), significant strong scattered standing waves are not found in the subregions between the adjacent digital modules even if the position b of the gap approaches the rightmost side. In addition, when the gap location b is 90 mm, stronger magnetic field intensities are observed at the right subregion in Region 4, unlike the case of Fig. 5. These differences are due to the different arrangement of the digital modules.

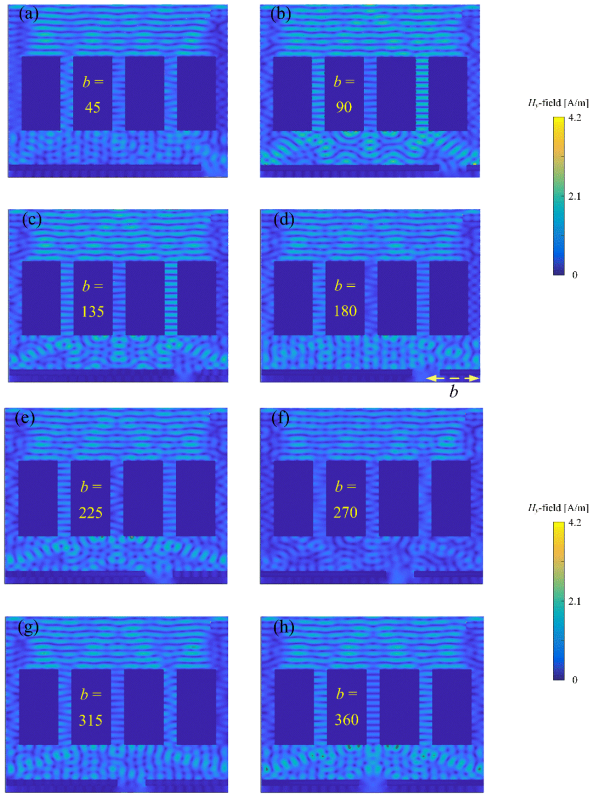

FIGURE 8. H_y-field distributions as a function of variable *b* (unit: mm) when TM_0 mode is incident, and the number of digital modules is four.

H_y-field intensities as a function of the gap location b are investigated as depicted in Fig. 9(a). In this case, the H_y-field intensities are captured along the line AB, as described in Fig. 9(b). The line AB is located between the two right digital modules, because relatively stronger magnetic fields are observed in the subregion. Stronger magnetic fields are formed when b approaches 90 or 135 mm, as shown in Fig. 9(a). On the contrary, the weakest magnetic field intensity is found when b is 270 mm, because a large portion of the incident wave passes through the subregions and exits into the gap of the rear door.

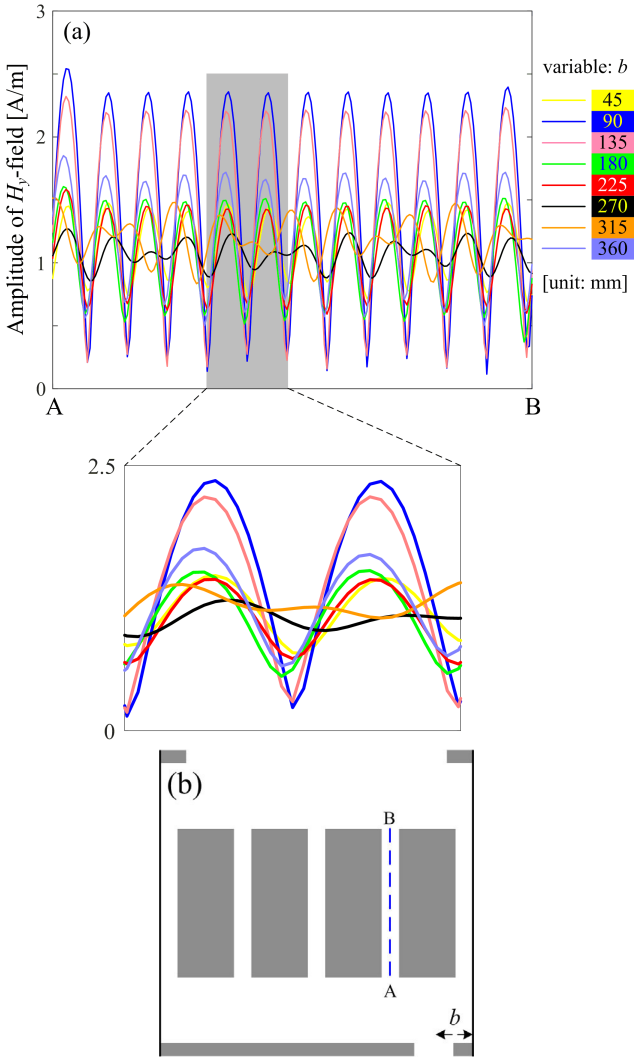

FIGURE 9. The H_y-field strengths along the line AB when *b* varies from 45 to 360 mm, and four digital modules in the cabinet are considered. (b) The position of the line AB is depicted in the cabinet.

The H_y-field intensities along the line CD, as shown in Fig. 10, are investigated as a function of b. As provided in Table 3, the average and maximum H_y-field

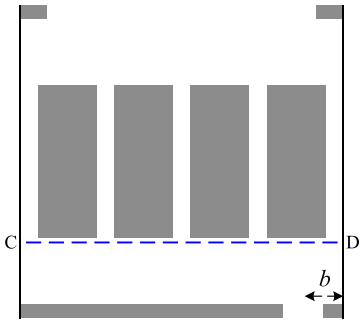

FIGURE 10. The line CD is described in the cabinet, and the H_y-field along the line is examined as a function of b. The average and maximum values along the line are presented in Table 3.

TABLE 3. Average and maximum H_y -field strengths along the line CD in Fig. 10 with respect to b.

b [mm]	Average values [A/m]	Maximum values [A/m]
45	1.038	2.236
90	1.197	2.774
135	1.184	2.716
180	1.334	2.895
225	1.336	3.365
270	0.922	2.043
315	1.184	2.604
360	1.409	2.911

intensities along the line CD are computed as a function of b. The strongest average H_y-field intensities are found when the location b becomes 360 mm (center of the rear door). In this geometry, relatively stronger standing waves are found in Region 5 because the incident wave does not transmit into the back of the cabinet and stays inside the cabinet. The maximum H_y-field intensity is obtained when b becomes 225 mm, while 2.043 A/m is calculated, when b is 270 mm, as given in the last column of Table 3, which shows clear difference between the two.

D. SCATTERED FIELDS FOR VARIOUS GAP WIDTHS IN THE REAR DOOR

Figs. 11(a) and (b) show the scattered magnetic field intensities along the line AB as a function of the gap width $2g_b$ when b is fixed at 90 and 315 mm, respectively. The number of digital modules inside the cabinet is three. In Fig. 11(a), similar field intensity patterns are observed along the line AB for all cases, except for $2g_b = 30$ mm. On the contrary, in Fig. 11(b), the strongest magnetic field intensities are observed when the gap width $2g_b$ becomes 30–60 mm. The wider the gap width $2g_b$, the weaker the scattered magnetic field intensities along the line AB.

Similar to Fig. 11, the scattered magnetic field intensities along the line CD are investigated, as described in Fig. 12. Table 4 provides the H_y-field intensities along the line CD as a function of the gap width $2g_b$ in the rear door examined when the gap position b is 90 mm. In this case, a relatively stronger magnetic field intensity is obtained when $2g_b$ becomes 30 mm. Stronger standing wave patterns

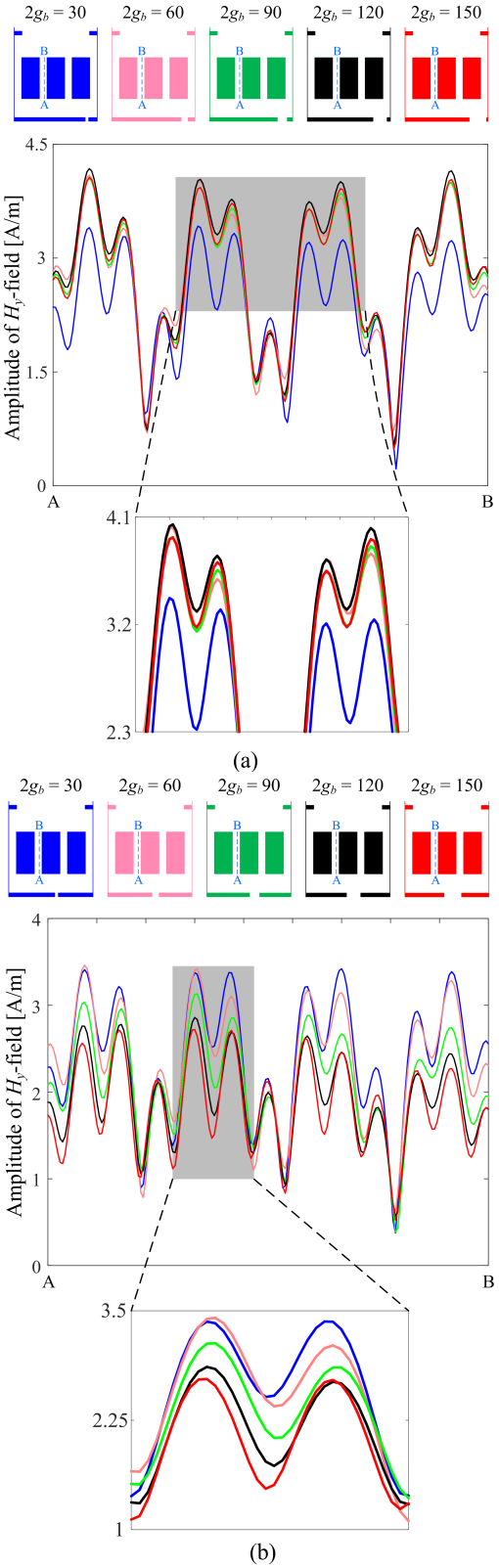

FIGURE 11. The H_y-field strengths along the line AB as a function of the gap width of 2 g_b when b is (a) 90 mm and (b) 315 mm, respectively. In both plots, $2g_b$ is changed to 30, 60, 90, 120, and 150 mm, respectively.

are observed, because the narrow gap width causes more confined electromagnetic fields in Region 5. Table 5 presents

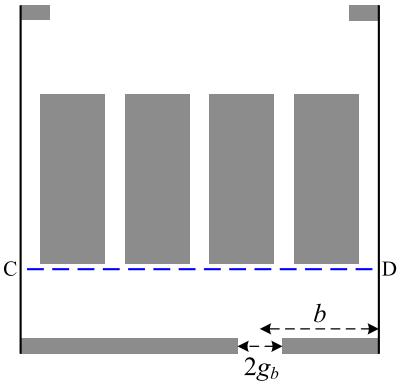

FIGURE 12. The line CD is described in the cabinet, and the H_y-field along the line is examined as a function of b and $2g_b$ when four digital modules are considered. The average and maximum values along the line are presented in Tables 4 and 5.

TABLE 4. Average and maximum H_y-field strengths along the line CD in Fig. 12 with respect to 2 g_b ($b = 90$ mm).

$2g_b$ [mm]	Average values [A/m]	Maximum values [A/m]
30	1.227	2.854
60	1.164	2.506
90	1.197	2.774
120	1.114	2.373
150	1.071	2.286

TABLE 5. Average and maximum H_y-field strengths along the line CD in Fig. 12 with respect to 2 g_b ($b = 225$ mm).

$2g_b$ [mm]	Average values [A/m]	Maximum values [A/m]
30	1.249	2.764
60	1.188	3.073
90	1.336	3.365
120	0.912	2.369
150	1.131	2.941

the H_y-field intensities when the gap position is 225 mm. In this case, the strongest H_y-field intensities along the line CD are formed when $2g_b$ is 90 mm, which shows a different tendency compared to the results provided in Table 4.

IV. VALIDATION OF THE MMT FORMULATION

The electric field intensity along the blue dashed line RP in Fig. 13(a) is obtained and compared to the results produced by the commercial software for the same geometry of the cabinet. The electric field intensity along the line RP is obtained when the number of digital modules is four. The power conservations at each junction are confirmed, and the electric field intensity along the line RP by the MMT matches well with the field intensity from the FEKO commercial software [15], as depicted in Fig. 13(b).

V. DISCUSSION

From the current research results as well as the results in Ref. [6] (when one bundle of digital module is considered), following points are concluded. (1) For the case of normally incident waves in parallel polarization, it is found that the

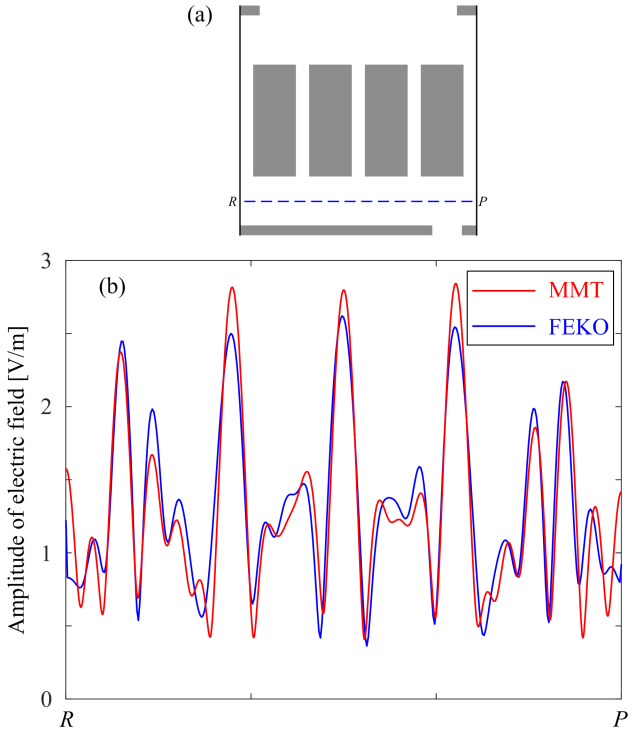

FIGURE 13. (a) The blue dashed line RP in the cabinet is depicted to observe scattered electric fields and (b) the validation of scattered electric fields along the blue line RP by the mode-matching technique (MMT; red solid line) and the FEKO commercial software (blue solid line) when TM_0 mode is applied.

strongest electromagnetic field intensities appear commonly at the subregions between adjacent digital modules (In [6], the subregion indicates the region between a digital module and side wall). (2) At these cases, the strongest magnetic field intensities are obtained approximately 4 [A/m] in common, when incident magnetic field intensity is 1 [A/m]. (3) Therefore, if the wave is incident into the cabinet, maximally 4 times incident magnetic fields are found between the digital modules. Therefore, it will be necessary to reflect these results to the electromagnetic interference (EMI) regulation.

VI. CONCLUSION

This paper investigated the scattering characteristics inside the cabinet of an NPP using the MMT when arbitrary wireless devices were assumed to be applied inside the NPP. The number of digital modules inside the cabinet and the small opening of the rear door of the cabinet were considered because these geometries were more realistic, whereas the previous research took account of a single block of modules and closed rear door of the cabinet. To apply multiple digital modules to the MMT, the modal decomposition was dealt with, and the multiregion problem was introduced because the entire scattering phenomena should be examined. The power conservation at each junction was computed and the results were validated; therefore, the overall scattering characteristics inside the cabinet could be systematically investigated. The scattering characteristics for three and four digital

module cases and as functions of the gap position or the gap width in the rear door of the cabinet were explained. In general, weaker scattered fields were found when the center of the gap in the rear door of the cabinet was located 360 mm away from the side wall for the three digital module case, while 270 mm for four digital module case. Finally, the scattered fields from our formulation were validated by the results produced by the FEKO commercial software, and it was confirmed that the results by the MMT formulation were appropriate. On the basis of these investigations, when determining the geometry of the cabinet and digital modules, the scattered field inside the cabinet is systematically analyzed in advance, and appropriate design guidelines for the cabinet can be suggested.

REFERENCES

[1] P. Keebler and H. S. Berger. (2011). *Managing the Use of Wireless Devices in Nuclear Power Plants*. [Online]. Available: https://incompliancemag.com/article/managing-the-use-of-wireless-devices-in-nuclear-power-plants/

[2] J. Blaney, "Benefit by installing reliable secure wireless communications networks at your plant," *Combined Cycle J.*, pp. 98–104, 3rd Quart., 2008.

[3] J.-E. Park, S. Youn, J. Choo, and H. Choo, "Indoor exclusion zone analysis in a nuclear power plant with wirelessHART application," *IEICE Electron. Exp.*, vol. 16, no. 10, pp. 1–6, 2019.

[4] J. Choo, J. Choo, and Y.-H. Kim, "Evaluation of electromagnetic interference from axially ruptured coaxial cable with multiple dielectrics used in nuclear power plants," *IEEE Trans. Electromagn. Compat.*, vol. 61, no. 3, pp. 860–869, Jun. 2019.

[5] J. Choo, C. Jeong, and J. Choo, "Transverse electric scattering of open cabinet in nuclear power plants," *IEEE Antennas Wireless Propag. Lett.*, vol. 15, pp. 1204–1207, 2016.

[6] J.-E. Park, J. Choo, and H. Choo, "Electromagnetic scattering of periodic cabinets in nuclear power plants: Parallel polarization," *IEEE Access*, vol. 7, pp. 16487–16493, 2019.

[7] J. Choo, J.-E. Park, H. Choo, and Y.-H. Kim, "Electromagnetic interference caused by parasitic electric-line current on a digital module in a closed cabinet," *IEEE Access*, vol. 7, pp. 59806–59812, 2019.

[8] J. Choo, J. Choo, and Y.-H. Kim, "Shielding effectiveness of open cabinet containing digital modules using ferrite sheet," *IEEE Trans. Magn.*, vol. 53, no. 12, Dec. 2017, Art. no. 2900609.

[9] J.-W. Rim and I.-S. Koh, "SAR image generation of ocean surface using time-divided velocity bunching model," *J. Electromagn. Eng. Sci.*, vol. 19, no. 2, pp. 82–88, Apr. 2019.

[10] S. M. Seo, "An IE-FFT algorithm to analyze PEC objects for MFIE formulation," *J. Electromagn. Eng. Sci.*, vol. 19, no. 1, pp. 6–12, Jan. 2019.

[11] J.-E. Park, F. L. Teixeira, and B.-H. Borges, "Analysis of deep-subwavelength Au and Ag slit transmittances at terahertz frequencies," *J. Opt. Soc. Amer. B, Opt. Phys.*, vol. 33, no. 7, pp. 1355–1364, 2016.

[12] A. Wexler, "Solution of waveguide discontinuities by modal analysis," *IEEE Trans. Microw. Theory Techn.*, vol. MTT-15, no. 9, pp. 508–517, Sep. 1967.

[13] S. Yoo, J.-E. Park, and H. Choo, "Resonant transmission through periodic subwavelength terahertz metallic slits based on a quartz plate," *Results Phys.*, vol. 16, Mar. 2020, Art. no. 102881.

[14] W. C. Chew, "Mode matching method," in *Waves and Fields in Inhomogeneous Media*. New York, NY, USA: Wiley, 1999, ch. 6, pp. 327–374.

[15] FEKO. (2019). *Altair*. [Online]. Available: http://www.altair.com

JONG-EON PARK received the B.S., M.S., and Ph.D. degrees from the School of Electrical Engineering and Computer Science, Kyungpook National University, Daegu, South Korea, in 2006, 2009, and 2013, respectively. From 2013 to 2015, he was a Postdoctoral Researcher with The Ohio State University. From 2016 to 2019, he was a Research Professor with Hongik University. Since 2020, he has been with Dongguk University, where he is currently an Assistant Professor with the Department of Safety Engineering. His research interests include scattering through aperture, antenna design, and computational electromagnetics.

HOSUNG CHOO (Senior Member, IEEE) received the B.S. degree in radio science and engineering from Hanyang University, Seoul, in 1998, and the M.S. and Ph.D. degrees in electrical and computer engineering from The University of Texas at Austin, in 2000 and 2003, respectively. In September 2003, he joined the School of Electronic and Electrical Engineering, Hongik University, Seoul, South Korea, where he is currently a Professor. His principal research interests include electrically small antennas for wireless communications, reader and tag antennas for RFID, on-glass and conformal antennas for vehicles and aircraft, and array antennas for GPS applications.